Non-isothermal crystallization kinetics of halloysite nanotube/short glass fibre-reinforced polypropylene composites

Malavika Reghunathan Kalathil[1] · R. B. Santoshi[1] · N. Rasana[1,2] · K. Jayanarayanan[1,2]

Abstract

The synergistic effect of multiscale fillers on the kinetics of non-isothermal crystallization of polypropylene (PP) reinforced with microscale glass fibres (GF) and nanoscale halloysite nanotubes (HNT) is investigated in this study. The glass fibre concentration is set at 20 mass% and that of HNT at 2.5 mass% in hybrid multiscale composites, and the crystallization kinetics of composites are analysed at different cooling rates. The lower critical free energy barrier for the formation of critical nuclei size and faster stable nuclei formation is determined for nano- and hybrid composites. The kinetics of crystallization for hybrid composite are best explained by Mo's model, while Avrami and Ozawa could explicate the kinetics of initial stages of crystallization. The dependence of effective activation energy on the extent of relative crystallization for micro-, nano- and hybrid composites was explored via Friedman model. The X-ray diffraction (XRD) analysis shows the ability of HNT to induce α and β crystals and the ability of multiscale fillers to reduce the crystal sizes without affecting the standard lattice planes of neat polypropylene.
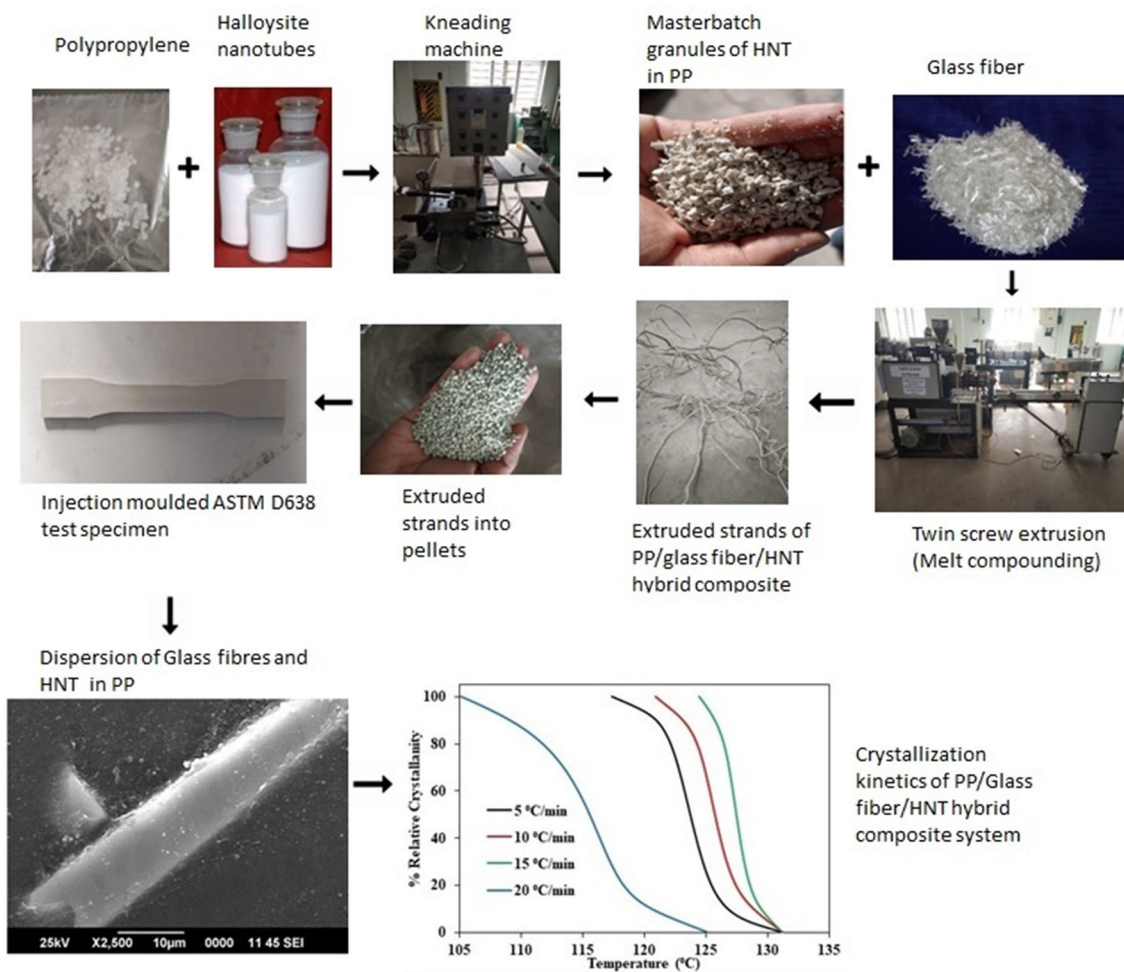
✉ N. Rasana
   n_rasana@cb.amrita.edu; rasana9@gmail.com

✉ K. Jayanarayanan
   kj_narayanan@cb.amrita.edu

1   Department of Chemical Engineering and Materials Science, Amrita School of Engineering - Coimbatore, Amrita Vishwa Vidyapeetham, Coimbatore, India

2   Centre of Excellence in Advanced Materials and Green Technologies (CoE-AMGT), Amrita School of Engineering - Coimbatore, Amrita Vishwa Vidyapeetham, Coimbatore, India

Graphical abstract

Polypropylene · Halloysite nanotubes → Kneading machine → Masterbatch granules of HNT in PP + Glass fiber → Twin screw extrusion (Melt compounding) → Extruded strands of PP/glass fiber/HNT hybrid composite → Extruded strands into pellets → Injection moulded ASTM D638 test specimen → Dispersion of Glass fibres and HNT in PP → Crystallization kinetics of PP/Glass fiber/HNT hybrid composite system

Introduction

Polypropylene (PP) is one of the largest used thermoplastic polymers, due to its large availability, low cost, ease of processing and excellent resistance to a wide range of acids and bases [1–4]. It has hence found applications in all sectors, ranging from household to commercial and industrial, like the automotive and packaging. Some of the inferior characteristics of PP include slow crystallization rate, high post-moulding volumetric shrinkage, low mechanical strength and increased flammability. The aforementioned shortcomings can be improved with the inclusion of fillers of various types and sizes like glass fibre (GF), carbon nanotube, nanosilica, nanoclay, graphene nanoplatelets, etc.

GF is usually added to PP as a microfiller. Campbell and Qayyum [1] indicated an increase in nucleation density when PP is accompanied by fillers. Further, in a study conducted by Gupta et al. [2] it was found that both the crystallization rate and the crystallinity of PP increased with the addition of GF. With the improvement in technology, the focus has also shifted to incorporating nano fillers in polymer matrices. Several researchers [3–5] have studied crystallization of PP with nanofillers like multi-walled carbon nanotube (MWCNT) and halloysite nanotubes (HNT) and have accomplished significant enhancement of mechanical and/or thermal properties. Many authors have explored the crystallization kinetics of various polymers with the inclusion of individual or dual nanoreinforcements [3, 5, 6]. Jenifer et al. [7] explored the non-isothermal crystallization kinetics of PP hybrid composite composed of micron-scale glass fibres and nanoscale halloysite nanotubes using differential scanning calorimetry(DSC) and several theoretical models. Enhanced peak crystallization temperature was reported for PP composites in

comparison with neat PP. Wang et al. [8] reported the drop in crystallization temperature (T_c) with enhanced cooling rate, and the generation of crystal imperfections. They noticed that at relatively lower temperatures owing to the weak mobility of polymer chains crystal imperfections are induced which is manifested by widened crystallization peaks [8].

Recently, the inclusion of naturally occurring fillers such as halloysite nanotubes (HNT) is increasingly becoming the focus of investigations owing to their high length-to-diameter (L/D) ratio, superior temperature-resistant properties, nanoscale lumens, low cost and large abundance [9]. These properties along with the fact that HNTs possess a lower density of hydroxyl groups on their surface when compared to other silicates makes it a potent reinforcement for polymers. According to a report by Jenifer et al. [7], PP when melt blended with HNTs and GF, in both the presence and absence of compatibilizer maleic anhydride (MAH), were shown to have enhanced thermal, flame and tensile properties. The tensile strength of PP was shown to have increased by 70.8% in the case of of dual reinforcement with HNT and glass fibre and 13.5% with HNT alone. Du et al. [10] discussed the excellent heterogeneous nucleating ability of HNTs in PP and evaluated activation energy for non-isothermal crystallization of PP phase using DSC studies and demonstrated the same using polarized light microscopy (PLM). The authors verified that PP/HNT nanocomposites exhibited higher crystallization rate and activation energy (ΔE_a) owing to the nucleation sites induced by HNT nanofillers. It was also revealed that HNTs have twin nucleating ability for the formation of α-iPP and β-iPP crystallites of PP phase, which was confirmed using XRD, scanning electron microscopy (SEM), DSC and polarized optical microscopy (POM) [11]. PP composite with 20 parts per hundred (phr) of HNT was found to generate maximum number of crystals and is strongly dependent on loading of HNTs. At lower cooling rate of 2.5 °C min^{-1}, the maximum content of crystals was obtained and such a formation of crystals is connected to the unique surface morphology of HNTs.

The non-isothermal crystallization behaviour of poly(butylene terephthalate) (PBT)/halloysite composites was investigated by Oburoğlu et al. [12] using DSC, XRD and dynamic mechanical analysis (DMA) tests. It was reported that while the Ozawa model perfectly fit the non-isothermal crystallization data of PBT, it failed to explain the kinetics of the composites. The results concluded from the DMA analysis explained the ability of HNT to enhance the elastic capability of the specimen owing to the restriction effects of HNTs on the PBT chains (filler–polymer interactive effects). From the activation energy studies, it was found that at higher contents of halloysite tubes, activation energy (ΔE_a) dropped which indicates the reduced energy barrier. Zhang et al. [13] concluded that the higher the E_a,

the higher the energy release during cooling and more difficult the mobility of chains during crystallization.

The dearth in the theoretical studies on the synergistic crystallization behaviour of multiscale composites with GF and HNTs is the inspiration behind this study to understand the crystallization kinetics of the nano- and multiscale composites. Since most of the industrial polymer processing operations occur under non-isothermal conditions, an effort has been made to investigate the influence of multiscale fillers on non-isothermal crystallization behaviour of PP using the kinetic models of Ozawa, Avrami, Mo, Chuah and Friedman models for comparison with the experimental results.

Experimental

Materials

The base polymer PP was procured from Reliance Industries Ltd., India (Repol H110MA, melt flow index and melting temperature: 11.0 g/10 min and 167.7 °C respectively). Glass fibres were obtained from Brakes India Ltd., India, of length 3 mm and diameter 10 μm. The halloysite nanotubes were purchased from Sigma-Aldrich, India, which was in the form of a white powder (surface area: 64 m^2 gm^{-1}, diameter and length varied from 30 to 70 nm and 1 to 3 microns, respectively).

Composite preparation

The masterbatch preparation was carried out in a laboratory scale internal mixer using PP and HNT. The PP along with desired amounts of masterbatch and glass fibre was then mixed in a tumble mixer and in the next step compounded using co-rotating twin screw extruder. The L/D ratio of the extruder barrel was 40:1, and the temperatures at different zones of the extruder ranged from 160 to 210 °C with increments of 10 °C from the feed zone till the die end. The screw speed was set at 75 rpm. The polymer strands were then quenched in a water bath and pelletized. These pelletized polymers were injection moulded (ASTM D 638) to form standard test specimens. The compositions chosen for our study are given in Table 1.

Table 1 Compositions of samples and nomenclature

Sample name	PP mass/%	GF mass/%	HNT mass/%
PP	100	0	0
PPG	80	20	0
PPGH	77.5	20	2.5
PPH	97.5	0	2.5

Characterization methods

Differential scanning calorimetry

Differential scanning calorimetry (DSC) was performed by a TA Instruments Q20 V24.10 Build 122 device under non-isothermal conditions. The test was performed by first heating the samples up to 200 ℃ holding there for 3 min to relieve the thermal stresses, and then cooling at various cooling rates of 5, 10, 15 and 20 ℃ min^{-1}. The DSC data obtained was used to study melting and crystallization characteristics and to predict the kinetics of crystallization using various theoretical models.

Transmission electron microscopy (TEM) and scanning electron microscopy (SEM)

TEM was carried out on prepared ultrathin slices of the PPH composites by a Japan Electron Optics Lab (JEOL)-JEM-2100 Transmission Electron Microscope at an acceleration voltage of 200 kV to reveal the dispersion of HNTs in the matrix. The surface morphology of the PPGH composites was analysed using a JEOL JSM-6490LA model make scanning electron microscope. Firstly, injection moulded samples were cut in the dimensions of 0.5 cm × 0.5 cm and treated with hot xylene and sputtered with gold–palladium of thickness less than 3 nm.

X-ray diffraction (XRD)

The wide-angle X-ray diffractometer used is the Rigaku Ultima IV, with the X-ray source being Cu, operated at 40 kV/30 mA at continuous scanning mode of 2θ from 5° to 80° with a step of 0.02° being used to identify the crystal lattice planes and degree of crystallinity.

Results and discussion

Microstructure analysis

The images in Fig. 1 are the TEM micrographs of the PPH specimen. Figure 1a shows the image at the scale of 100 nm. The tube-like structure of HNT is vivid, and its dispersion in the polymer matrix can be clearly seen in Fig. 1b. Figure 1c suggests non-uniform dispersion with slight agglomerations of HNT. The obvious reason could be the van der Waal's force of attraction between the nanotubes [6]. Another possibility of agglomeration is the reduction in the length of some of the nanotubes due to mechanical attrition. The attrition and abrasion of the nano- and microfillers usually happen during

the high shear mixing process which is an extremely important factor determining the quality of mixing. It includes two processes, namely (1) distributive mixing done to ensure an even distribution of the fillers in the PP matrix and is achieved by providing convoluted flow paths that repeatedly split and reorient the flow and (2) dispersive mixing to increase the dispersion of the distributed fillers, i.e. it prevents agglomeration of the fillers which can be achieved by passing the hot polymer melt compound through small regions of intense deformation. It involves generating high stresses to break the agglomerating tendency of the nanofillers. Upon the introduction of HNT in the GF-filled PP matrix, the high aspect ratio of HNT makes it wrap around neighbouring glass fibres and hold it in place firmly. The PP chains also tend to wrap around the HNTs tightly due to its nanoscale than on microscale glass fibres [7]. Figure 1d and e shows the SEM image of PPGH multiscale hybrid composite. Figure 1d represents a single glass fibre zoomed out of uniformly dispersed glass fibres in the matrix. The distribution of HNTs on the cylindrical surface of glass fibre and in the neighbouring regions in PP matrix is evident. The HNTs dispersed could be observed as white spherical spots and projections from PP matrix. The SEM images of PPG and PPH composites are included under section S1 (Fig. S1a, b) which also confirm the dispersion and distribution of glass fibres and HNTs in virgin PP matrix.

### Non-isothermal crystallization

The crystallization process is a 3-step process where primary nucleation involves the largest specific surface area and is followed by secondary and ultimately by tertiary nucleation [14, 15]. As non-isothermal crystallization is one that takes place under continuous cooling with temperature varying as a function of time, the kinetics of crystallization depend on the instantaneous conditions that lead to the formation of spherulitic structures as well as the rate of the process. In a thermodynamic sense, it occurs during cooling below the melting temperature, at which time, crystals are at a lower free energy state than the liquid melt. The spontaneity of crystallization depends on ΔG [15]. Lower the ΔG, higher is the spontaneity. For a spherical nucleus of radius r, ΔG is given by Eq. (1) [15],

$$\Delta G = \frac{4}{3\pi r^3 \Delta G_c} + 4\pi r^2 \gamma^* \tag{1}$$

where ΔG_c is the free energy of crystallization/unit volume and γ^* specific surface free energy. During the crystallization process, as the cooling of the melt proceeds, ΔG initially increases, reaching a maximum, and then starts to decrease and reaches a stable value. The free energy and the radius at the maximum are represented by ΔG^* and r^*, and are called critical free energy barrier and critical size, beyond which ΔG decreases, producing a stable nucleus.

Fig. 1 a–c The TEM images of HNT-reinforced PP nanocomposite (PPH) at 100, 50 and 20 nm scales. **d** SEM image of glass fibre and HNT-reinforced PP hybrid composite (PPGH) **e** SEM image of PPGH hybrid composite showing the dispersion of HNTs on the surface/edges of glass fibre and in the PP matrix
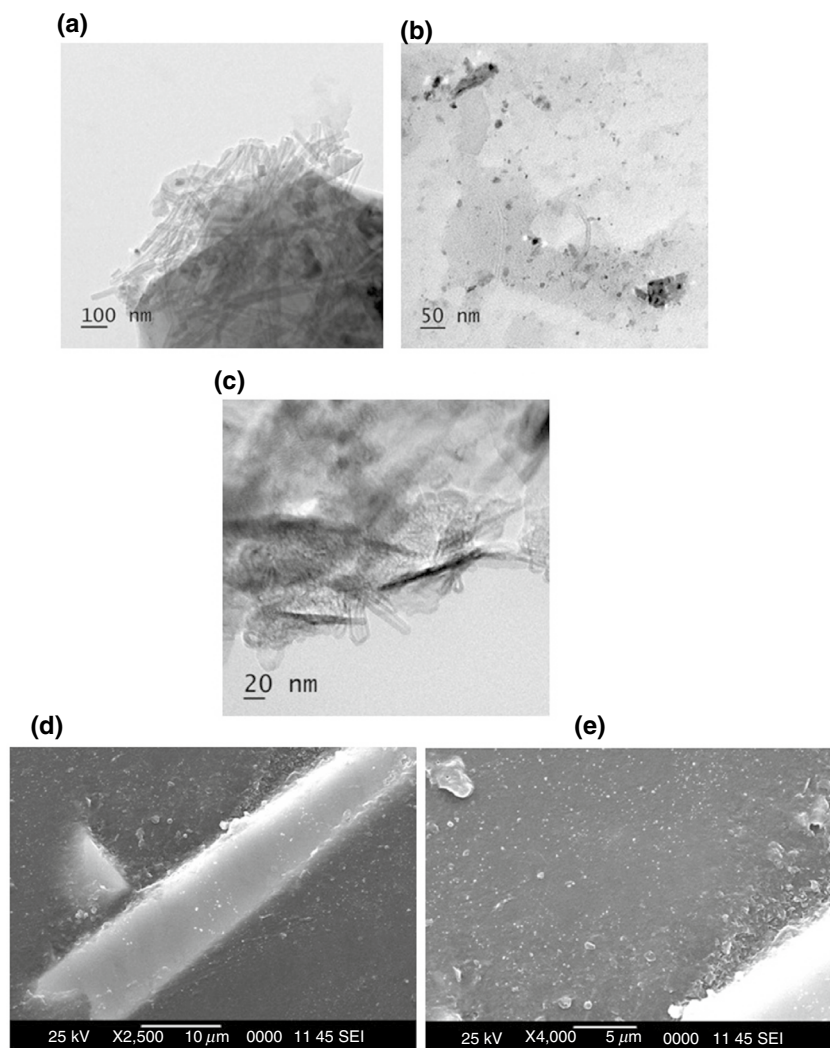

The cooling (Fig. 2a–d) and heating (Fig. S2e–h) curves were obtained from the DSC data. The range for DSC heating curves was taken as 120 °C to 180 °C and cooling curves was taken as 130 °C to 100 °C and all the samples were analysed with different cooling rates such as 5, 10, 15 and 20 ℃ min^{-1}. A wide range of crystallization parameters can be estimated from the DSC curves, including the onset temperature (T_o), endset temperature (T_e), peak crystallization temperature (T_c). The enthalpy of crystallization is used in the calculation of absolute percentage crystallinity. The important thermal properties obtained from DSC data are given in Table 2, and time parameters are reported in Table S1.

The degree of supercooling ($T_U = T_m - T_c$) decides the ease of formation of crystals from the molten state [16, 17]. If the difference ($T_m - T_c$) is low, then crystallization happens quickly and thus the process is less energy intensive, and vice versa. It was observed that PP has the highest T_U values and it reduces as fillers are added. This proves that heterogeneous crystallization takes place. At every cooling rate, T_o and T_c values enhanced with the addition of fillers. This is indicative of heterogeneous nucleation in hybrid and nanocomposites, thus initiating crystallization earlier than in neat PP.

For a given cooling rate, T_U decreases with the addition of fillers. PPGH and PPH have the lowest T_U in comparison with microcomposites and hence have the lowest ΔG^* and r^*. As a result, the critical free energy barrier and the critical size can be crossed quickly and can be seen in the small $t_{\left(\frac{1}{2}\right)}$ values of nano- and hybrid composite. Although T_U of PP is relatively high, only homogeneous crystallization takes place. The half time of crystallization ($t_{\left(\frac{1}{2}\right)}$) is the time taken for the 50% of the crystallization process to occur [6, 18–21]. The parameter half time is often used to evaluate the rate of crystallization [22]. A large $t_{\left(\frac{1}{2}\right)}$ implies a slow crystallization process and vice versa [23, 24]. The parameter t_{max} is the time taken to reach peak crystallization [22]. A low value of t_{max} implies

Fig. 2 DSC cooling curves of **a** PP, **b** PPG, **c** PPH, and **d** PPGH at the four different cooling rates. Cooling rates corresponding to each curve: Black line: 5 ℃ min^{-1}, red line: 10 ℃ min^{-1}, green line: 15 ℃ min^{-1} and blue line: 20 ℃ min^{-1}. (Color figure online)
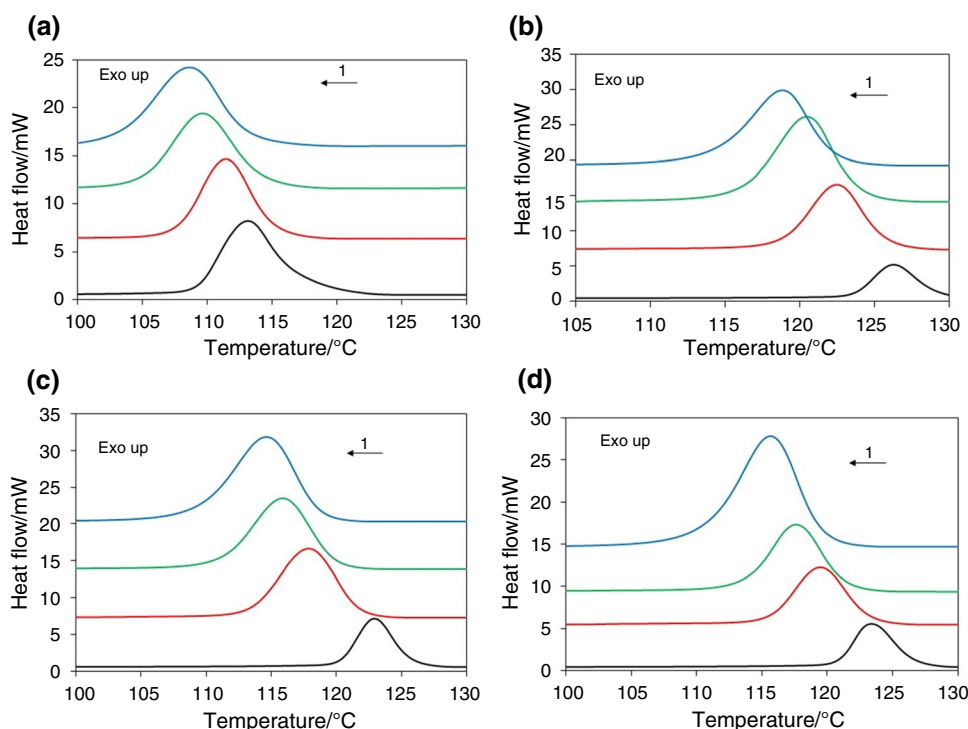
Table 2 Thermal properties of virgin PP, nano- (PPH), micro- (PPG) and hybrid composites (PPGH) obtained from DSC data

Specimen	Cooling rate R/ ℃ min^{-1}	Onset temperature T_o/℃	Endset temperature, T_e/℃	Peak crystallization temperature T_c/℃	Peak melting temperature T_m/℃	Degree of supercooling T_U/℃	Enthalpy of melting ΔH_m/ J g^{-1}	Enthalpy of crystallization ΔH_c/J g^{-1}
PP	5	128.2	105.3	113.1	167.2	54.0	115.0	81.5
	10	121.0	103.0	111.4	164.9	53.4	73.4	90.6
	15	120.0	102.1	109.6	165.2	55.6	55.5	78.8
	20	120.0	99.0	108.6	165.6	57.0	55.6	70.4
PPG	5	134.0	110.5	126.3	165.1	38.8	59.9	88.4
	10	134.0	108.4	122.5	165.7	43.2	70.6	103.0
	15	127.1	105.3	120.5	165.7	45.2	70.6	101.9
	20	125.5	102.7	118.9	165.1	46.2	49.3	74.2
PPGH	5	131.2	117.4	123.4	165.2	41.9	72.2	100.5
	10	128.2	111.8	119.5	166.5	47.0	55.9	84.2
	15	126.4	109.8	117.6	166.1	48.5	50.2	70.5
	20	125.1	105.2	115.6	166.6	50.9	50.6	97.1
PPH	5	130.3	118.1	122.9	165.2	42.29	95.64	133
	10	126.0	110.5	117.9	165.7	47.77	100.5	131.7
	15	124.5	108.1	115.9	164.6	48.72	71.74	94.3
	20	123.6	105.5	114.63	165.5	50.87	64.4	97.3

that peak crystallization is achieved faster. The width Δw is defined as the half width of the crystallization peak [16, 24].

$$\Delta w = T_o - T_c \quad (2)$$

From Table S1, it is observed that $t_{\left(\frac{1}{2}\right)}$ values decrease with increase in cooling rate for every composite because crystallization occurs faster. For a given cooling rate, $t_{\left(\frac{1}{2}\right)}$ is the least for PPH. Δw, half width of crystallization peak values for composites is low at high cooling rates because

of narrow peaks observed in the crystallization process, meaning that crystallization is quick. The relative crystallinity of a polymer matrix is dependent on crystallization time as well as the crystallization temperature as described in Eqs. (3) and (4) [18, 24–27].

$$X_c(T) = \frac{\int_{T_o}^{T} \frac{dH}{dT} dT}{\int_{T_o}^{T_e} \frac{dH}{dT} dT} \qquad (3)$$

$$X_c(t) = \frac{\int_{t_o}^{t} \frac{dH}{dt} dt}{\int_{t_o}^{t_e} \frac{dH}{dt} dt} \qquad (4)$$

where t is time and T is temperature and H is the heat flow. T ranges between T_o and T_e, and t between t_o and t_e.

Absolute crystallinity (X_c) is calculated from the melting and crystallization enthalpies obtained from the DSC data, using the formula (5) [28]

$$\frac{\Delta H_m - \Delta H_C}{\Delta H_m^0} \times 100 = X_C \qquad (5)$$

ΔH_m^o is defined for pure, 100% crystalline polymer. For PP, it is 207.1 J g^{-1} [28]. ΔH_m and ΔH_c are enthalpy of melting and enthalpy of crystallization, respectively. The calculated values of absolute crystallinity are given in Table S1.

The general trend observed is: with increase in cooling rate, X_c drops. This can be attributed to the insufficient time for the crystals to form completely as the mobility of the polymeric chains is hindered. It is noticed that at high cooling rates, multiscale and nanocomposite specimens are able to retain high absolute crystallinity values. The anomaly of PPH having lower absolute crystallinity can be explained by agglomeration of the fillers and also explained by the low Z_c values in the Avrami model in Sect. "Avrami model".

Avrami model

The model works on the assumption of constant crystallization temperature and can be used to describe the primary stages of non-isothermal crystallization and is given as in Eq. (6) [22, 29]

$$X_t = 1 - \exp(-Zt^n) \qquad (6)$$

where X_t is the relative percentage of crystallinity at time t, Z is the crystallization rate constant involving both nucleation and growth rate parameters, and n is the Avrami exponent that depends on the crystal growth mechanism, type of nucleation and crystal dimensions [12, 27, 30]. Z is also referred to as the bulk crystallization constant. Once linearized, the equation [12, 27, 30, 31] reduces to

$$\log(-\ln(1 - X_t)) = n\log t + \log Z \qquad (7)$$

where log Z and n can be found from the intercept and slope, respectively, of plots of $\log(-\ln(1 - X_t))$ versus t. Z is dependent on the shape of the growing crystallites, amount and type of nucleation and n is dependent on the growth geometry and type of nucleation. In the case of non-isothermal crystallization, Z and n do not have the same physical significance as in isothermal crystallization as there is a constant change in temperature under non-isothermal condition. This affects the rates of both nuclei formation and spherulite growth since they are temperature dependent. In order to apply the Avrami equation to the non-isothermal crystallization process and eliminate the effect of the cooling rate, it was modified by Jeziorny [31] to the equation below, where Z_c is the Jeziorny crystallization constant.

$$\log Z_c = \frac{\log Z}{R} \qquad (8)$$

From the plots in Fig. 3, it is observed that the curves at higher cooling rates maintain linearity than the curves at lower cooling rates. In all cases, the curves are linear to an appreciable extent only in the earlier stages of crystallization and deviate in the later stages, thus signifying the inability of the Avrami equation to explain the secondary stage of crystallization. However, both the Avrami and Jeziorny constants have been estimated using the linear portion of the curves and are given in Table S2. There is an increasing trend in the value of Z_c with an elevation in the cooling rate. In the case of higher cooling rates, melt crystallization shifts to low temperatures which leads to higher undercooling and higher crystallization rate. Both Z_c and n are found to increase with the addition of fillers even at the same cooling rate, explaining the effect of heterogeneous nucleation due to the addition of fillers. The decrease in n and Z_c in PPGH when compared to PPH could be assumed to occur due to an aggregation of the fillers in PPGH. The aggregation leads to a decrease of the nucleation ability of the filler since the number of heterogeneous nuclei sites decreases [32].

The significance of this model lies in the Avrami constants. Muller et al. [33, 34] explained that Avrami constant 'n' ($n = n_{gd} + n_n$) can be expressed as the contribution of two terms (1) dimensionality of the growing crystals (n_{gd}) and (2) time dependence of nucleation rate (n_n). The term (n_{gd}) can take only integer values 1, 2 and 3 representing one-, two- and three-dimensional entities. The $n_{gd} = 2$ shows two-dimensional lamella structures and $n_{gd} = 3$ represents spherulitic 3-D crystallite structure. The parameter n_n can take values between 0 and 1 which corresponds to instantaneous nucleation and sporadic nucleation, respectively. Mostly nucleation could not be 100% instantaneous and sporadic and hence n_n lies between 0 and 1. An axialitic morphology that nucleated instantaneously takes n value of 2. Since the n values of the composites lies between 2.2 and

Fig. 3 Avrami plots of $\log(-\ln(1 - X_t))$ versus $\log t$ at various cooling rates for **a** PP, **b** PPG, **c** PPH, **d** PPGH. Cooling rates corresponding to each curve: black line: 5 ℃ min^{-1}, red line: 10 ℃ min^{-1}, green line: 15 ℃ min^{-1} and blue line: 20 ℃ min^{-1}. (Color figure online)
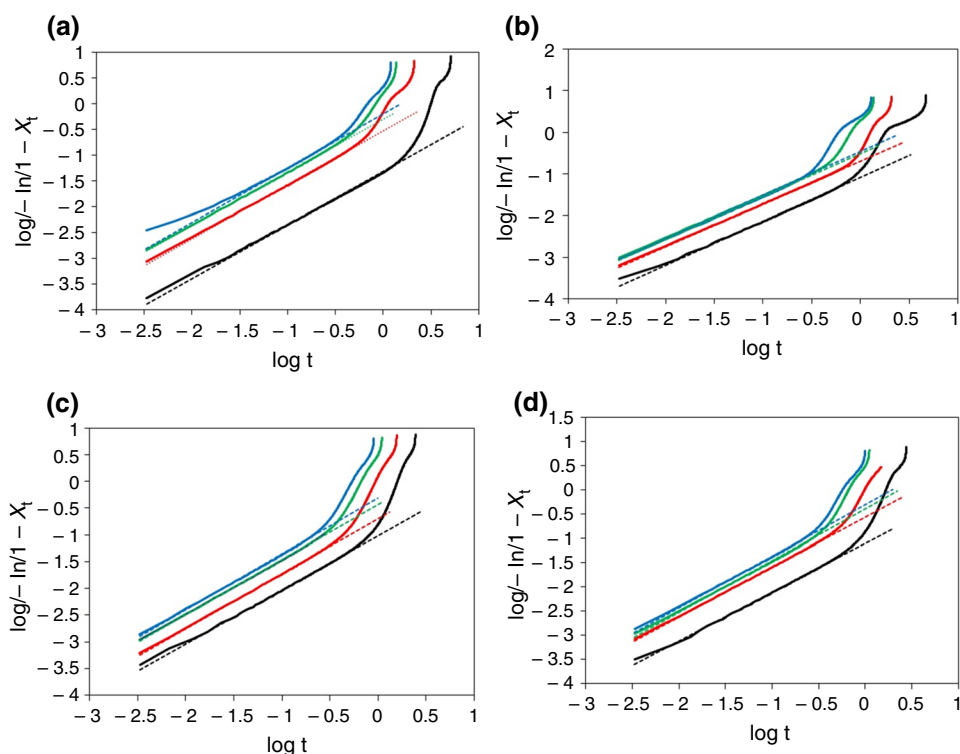
3.1, the growth mechanism is a combination of 2-D lamella structures and 3-D spherulites [35, 36]. Table S2 shows that the n values obtained for this study are 1.895, 2.235, 3.089, and 2.84 for PP, PPG, PPGH and PPH, respectively. Since the filled specimens have undergone thermal nucleation with nucleation being the rate determining step, it can be concluded that the possible crystal geometry takes up spherulitic structures [18, 35]. In general, higher values of Z_c, and n values close to 3 explain heterogeneous nucleation followed by 3-dimensional growth, which is clearly seen in PPGH hybrid multiscale composite [37–39].

Ozawa model

The model is based on the assumption that the mechanism is the same as the KAE (Kolmogorov Avrami Evans) model and it considers the non-isothermal crystallization process to be the sum of numerous infinitesimal isothermal crystallization processes. The Ozawa model is represented in Eq. (9) [19, 22, 40]

$$X_t = 1 - \exp\left(\frac{-K(T)}{R^m}\right) \tag{9}$$

where X_t is the relative crystallinity and can be obtained from the DSC data, $K(T)$ is the cooling crystallization function, R is the cooling rate constant, and m is the Ozawa exponent which depends on dimensions of crystal growth and

mechanism [10]. After taking double logarithms on both sides, the equation can be linearized into the form

$$\log(-\ln(1 - X_t) = \log K(T) - m\log R \tag{10}$$

where the slope and intercept are m and $\log K(T)$, respectively.

Figure 4 represents Ozawa plots for each of the four samples at different temperatures between the onset and the endset. It is observed from the plots that linearity is not exhibited in any of the curves, corresponding to composites. The absence of linearity is vivid as temperatures get lower or approaches endset, thus showing the inability of the model to explain the secondary stages of crystallization [41].

It is concluded that the plots at relatively higher crystallization temperatures are linear over a wide range of cooling rates, the reason being the slow crystallization and difficulty of entering into the secondary stage. It can also be noted that at a specific temperature, the crystallization process is at different stages for different cooling rates. While the plots tend to be more linear towards the start of the process for higher cooling rates signifying that the crystallization process is at an earlier stage, for lower cooling rates the crystallization process takes place towards the end or a later stage only [30]. Accordingly, as m does not remain constant with temperature, the experimental data do not fit the linearized equation throughout and this suggests that the Ozawa model cannot satisfactorily explain
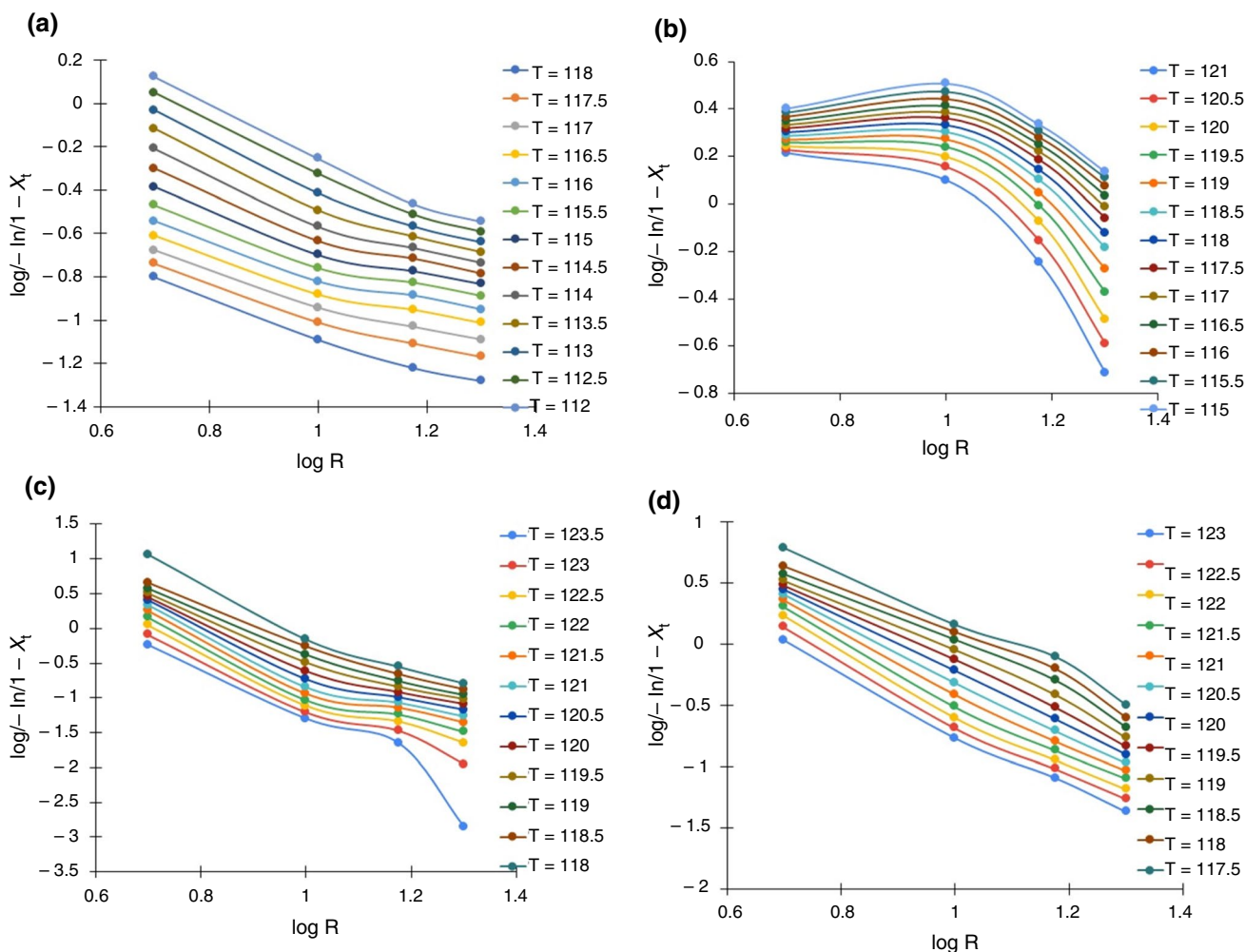
(a)

(b)

(c)

(d)

Fig. 4 Ozawa plots of $\log\left(-\ln\left(1 - X_t\right)\right)$ versus $\log R$ at various cooling rates for **a** PP, **b** PPG, **c** PPH and **d** PPGH

the non-isothermal crystallization behaviour of PPG microcomposite and PPH nanocomposite. Ozawa model could best fit with the crystallization kinetics exhibited by hybrid PPGH composite.

Mo model

The Mo model was formed by combining the Avrami and Ozawa models, to result in the expressions (11) and (12) [42–44]

$$\log Z + n\log t = \log(K(T)) - m\log R \tag{11}$$

$$\log R = \log(F(T)) - \alpha\log T \tag{12}$$

where R is the cooling rate, $\alpha = \frac{n}{m}$, $F(T)$ is the ratio of the Avrami exponent n to the Ozawa exponent m, and

$$F(T) = \left(\frac{K(T)}{Z}\right)\frac{1}{m} \tag{13}$$

$F(T)$ refers to the cooling rate that should be taken to obtain a particular level of crystallinity in a certain time. From the linearized plot of $\log R$ versus $\log t$, the value of $F(T)$ and a can be obtained from the intercept and the slope of the line, respectively, to an appreciable extent.

Additionally, from the plots in Fig. 5, it is visible that slower cooling rates result in longer duration for crystallization and the linearity of the plots suggests that Mo's model explains both stages of the non-isothermal crystallization process to an appreciable extent. Table S3 reports the parameters calculated using Mo's model for this study. $F(T)$ represents the difficulty in the crystallization process, and generally with an increase in relative crystallinity there is an increase in $F(T)$ [21, 22], implying, to obtain a higher degree of crystallinity, a higher cooling

Fig. 5 Mo plots of log R versus log t at varying percent relative crystallinity for **a** PP, **b** PPG, **c** PPH and **d** PPGH composite. Percent relative crystallinity: blue dots: 10%, red dots: 30%, yellow dots: 50%, green dots: 70%, orange dots: 90%. (Color figure online)
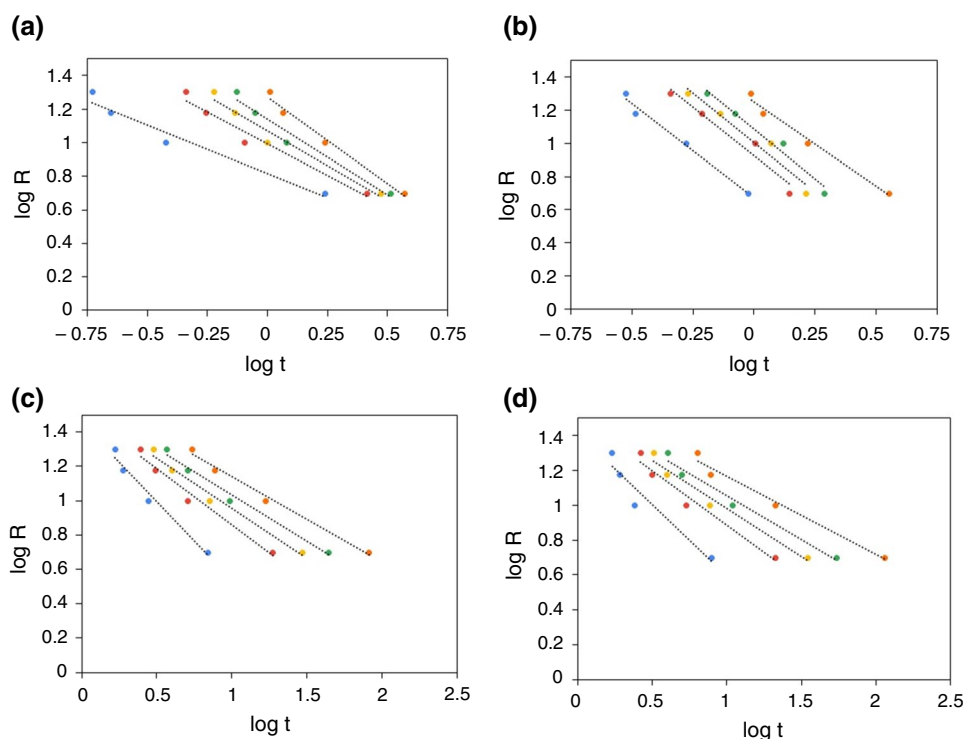
rate should be used [10]. The smaller values of $F(T)$ in the case of nanocomposites indicate the promotion of crystallization by the fillers; hence, a lower cooling rate can be used to attain that level of crystallinity. For a certain level of crystallinity, a higher value of $F(T)$ can represent the necessity for a higher cooling rate which relates to the possibility of a complex crystallization process [45], as is in the case of PPGH.

A decreasing trend in α depicts a faster crystallization rate, and this is visible in the case of the nanocomposite (PPH) and multiscale composite (PPGH). In PPG, there is an increasing trend in α which can be attributed to spherulitic impingement, hence lowering the crystallization rate. This effect seems to be countered by the inclusion of HNTs as observable from the α trend in PPGH and PPH. While neat PP has lower α values as compared to the composites, the further decrease in some of the composite samples is attributed to the complexity of crystal geometry. As fillers were incorporated into PP, the n values are higher for composites as was seen in the Avrami analysis and thus α for the composites, being a ratio of n to m is relatively higher compared to neat PP. Hence, the presence of fillers has enhanced the crystallization rate and the high values of R^2 shows that the experimental data fits the linearized equation fairly well.

Chuah model

The Ozawa model was developed as an extension of the Avrami model for the non-isothermal crystallization processes. However, the Ozawa model provides a result that is restricted to a definite set of temperatures and the corresponding relative crystallinity data. Another shortcoming of the Ozawa model is that it only describes the primary stage of crystallization that occurs before crystal impingement [46]. The model proposed by Caze et al. [47] was based on the assumption that the cooling crystallization function $K(T)$ varies exponentially with T upon cooling. Nevertheless, this model could only accurately explain the kinetics of cooling rate $R < 10\ {}^{\circ}\text{C}\ \text{min}^{-1}$. The Chuah model was developed to overcome the disadvantages of the Ozawa and the Caze model. The first step is to calculate the volume fraction of the crystals at every point of the crystallization process using the below given Eq. (14) [17, 22].

$$X_{\text{v}} = \frac{X_{\text{w}}\left(\frac{\rho_{\text{a}}}{\rho_{\text{c}}}\right)}{\left(1 - \left(1 - \frac{\rho_{\text{a}}}{\rho_{\text{c}}}\right)X_{\text{w}}\right)} \tag{14}$$

where X_{w} is the relative crystallinity calculated from the area under the DSC graph, and ρ_{a}, ρ_{c} are the bulk densities of the amorphous and crystalline parts of the polymer matrix and X_{v} is the crystal volume fraction. The effect of temperature on the ratio $\frac{\rho_{\text{a}}}{\rho_{\text{c}}}$ is given by Eq. (15) [48]:

$$\frac{\rho_{\text{a}}}{\rho_{\text{c}}} = \frac{\rho_{\text{a0}}}{\rho_{\text{c0}}}\exp\left[\left(T - T_r\right)\left(\alpha_{\text{c}} - \alpha_{\text{a}}\right)\right] \tag{15}$$

where the subscript 0 refers to reference temperature T_r that is taken to be 298 K, α_{c} and α_{a} are the thermal expansion

coefficients of the pure amorphous and crystalline states of the polymer which are obtained using the empirical relations $\alpha_a T_g = 0.16$ and $\alpha_c T_m^0 = 0.11$, suggested by Boyer-Spencer and Bondi [49]. Here, T_m^0 is the equilibrium melting temperature and T_g is the glass transition temperature of the polymer. Using the above-mentioned equation, Chuah et al. [46] proposed that

$$\ln\left[-\ln\left(1 - X_v\right)\right] = \alpha(T - T_q) \tag{16}$$

where α is the slope and T_q is the intercept of the curves plotted between $\ln\left[-\ln\left(1 - X_v\right)\right]$ and T (Fig. 6). A second graph of $\ln q$ versus T_q is plotted (Fig. 7) where q is cooling rate of the samples which predicts the cooling rate at which better alpha and crystallization pattern could be observed. Chuah parameters evaluated are reported in Table S4. Nucleation parameters obtained from Lauritzen–Hoffmann (L–H) model are included under Section S7.

Friedman model

Crystallization of a polymer matrix is impacted by two main factors—one being the free energy barrier of nucleation that
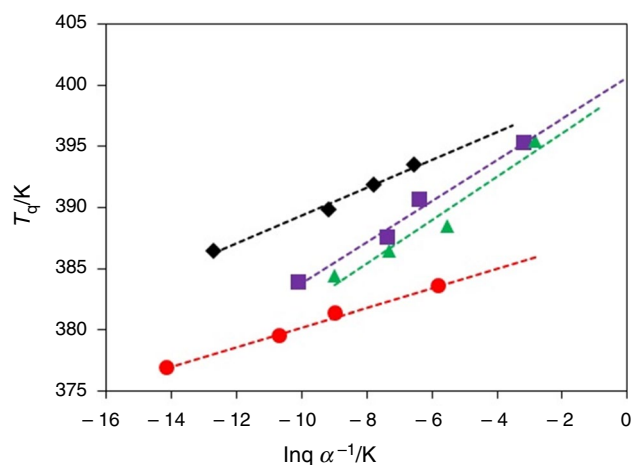
Fig. 7 Chuah plot of $\ln q$ α^{-1} versus Tq. Red dotted curve refers to PP, black diamond marker curve refers to PPG, green triangle curve refers to PPH, and purple square curve refers to PPGH composite. (Color figure online)

was explored before and the other being the effective activation energy (E_a) of the composites. The Kissinger and Friedman models are widely used in the non-isothermal
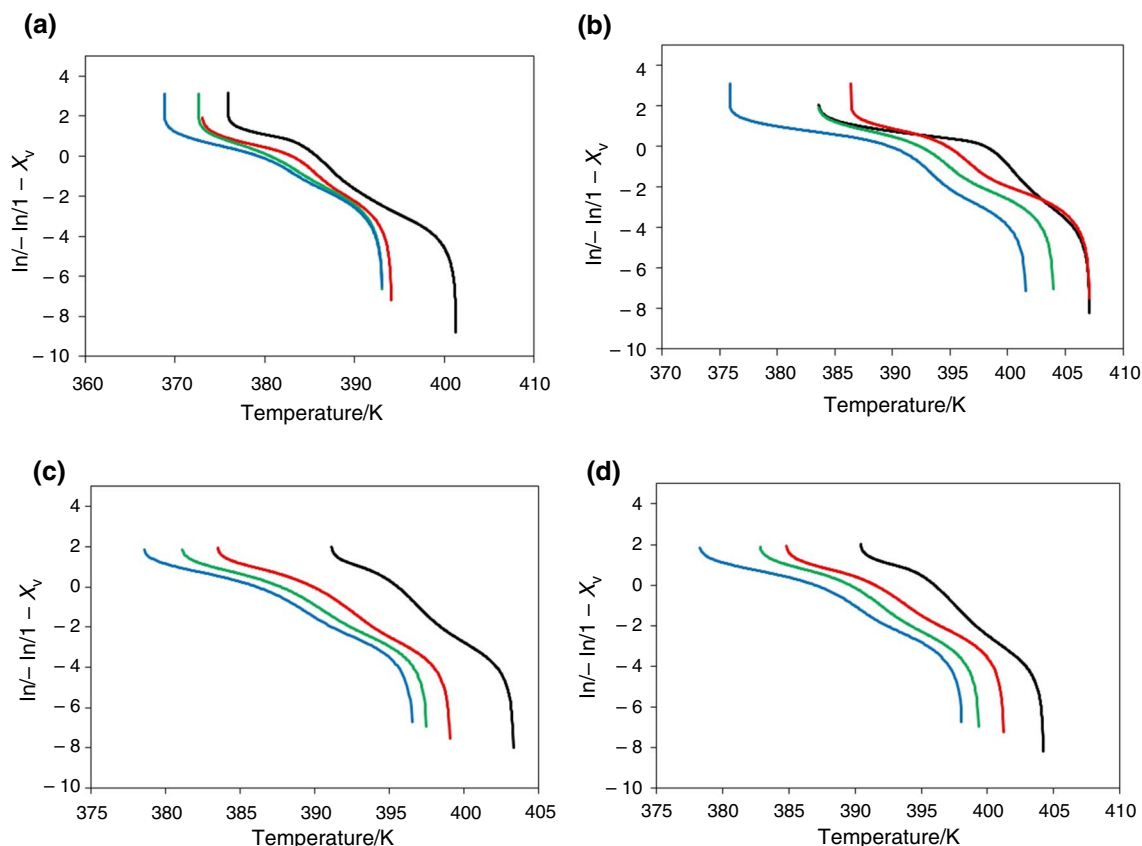
Fig. 6 **a–d** are the Chuah plots of $\ln\left(-\ln(1 - X_v)\right)$ versus T for PP, PPG, PPH and PPGH, respectively. Cooling rates corresponding to each curve: Black line: 5 ℃ min⁻¹, red line: 10 ℃ min⁻¹, green line: 15 ℃ min⁻¹ and blue line: 20 ℃ min⁻¹. (Color figure online)

crystallization kinetic studies of polymer composites to determine the activation energy; however, the Kissinger model has limitations due to it being a peak evolution method that does not describe the dependence of E_a on extent of crystallization and temperature [50]. The isoconversional method of Friedman is considered a better alternative in the view of recent literatures, as it evaluates the effective activation energy for every degree of crystallinity and the equation is as follows [50–52].

$$\ln\left(\frac{\mathrm{d}X}{\mathrm{d}t}\right)_{X,i} = A - \frac{\Delta E_X}{RT_{X,i}} \quad (17)$$

where $\left(\frac{\mathrm{d}X}{\mathrm{d}t}\right)$ is the instantaneous crystallization rate at a given degree of crystallinity X and cooling rate i, ΔE_X is the effective activation energy at a given X, R is the universal gas constant, and $T_{X,i}$ is the corresponding temperature related to X at different cooling rates.

It should be noted that here, E_a is determined as the temperature-dependent relative contribution of the mass transport and nucleation processes to the crystallization growth rate. Hence in this context, it is understood as overall effective activation energy ΔE_X rather than the value representing the magnitude of the energy barrier [53].

According to the Friedman method, at a certain cooling rate, the instantaneous crystallization rate $\left(\frac{\mathrm{d}X}{\mathrm{d}t}\right)$ is calculated by differentiating X with respect to time. Then by selecting various degree of crystallinity from 10 to 80%, the appropriate values of $\left(\frac{\mathrm{d}X}{\mathrm{d}t}\right)$ at that specific X, are correlated with corresponding crystallization temperature T_X. It can be seen from the equation that a straight line must be obtained by plotting $\ln\left(\frac{\mathrm{d}X}{\mathrm{d}t}\right)$ versus $\left(\frac{1}{T_X}\right)$ at different degrees of relative crystallinity X, the slope of which is equal to $\frac{-\Delta E_X}{R}$. The effective activation energy can hence be found. The plot of $\ln\left(\frac{\mathrm{d}X}{\mathrm{d}t}\right)$ versus $\left(\frac{1}{T_X}\right)$ for the hybrid composite PPGH for relative crystallinity percentages of 10–80 is given in Fig. 8. Kissinger plots (Fig. S3) for the determination of activation energy are reported under section S6. Friedman plots for PP, PPG and PPH are presented in Fig. S5, S6 and S7.

Additionally, the dependence of effective activation energy on the extent of relative crystallization for all the samples PP, PPG, PPGH and PPH is given in Fig. 9 and the results are listed in Table 3. From this plot, it is observed that for all the samples, ΔE increases with increase in relative degree of crystallinity from 10 to 80% except for PPG where there is a dip in the activation energy for $X > 60\%$. Considering this region of melt crystallization, with all samples ΔE is greatly negative at low degrees of crystallinity which corresponds to temperatures closer to the melting point [54]. Higher values of ΔE for higher fractions of crystallization suggest that crystallization in the initial stages was more
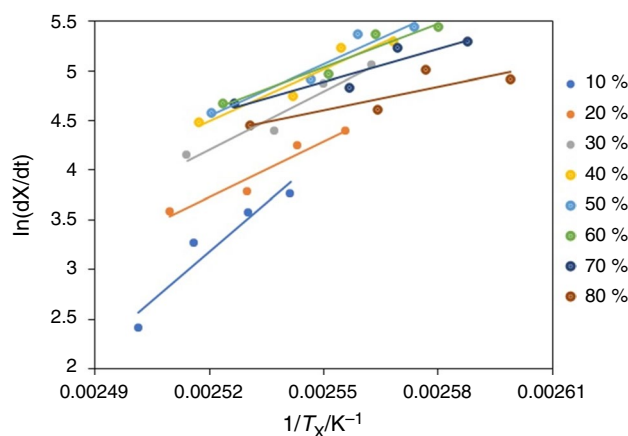
Fig. 8 Friedman plot of $\ln\left(\frac{\mathrm{d}X}{\mathrm{d}t}\right)$ for PPGH at % relative crystallinity from 10 to 80 for different cooling rates
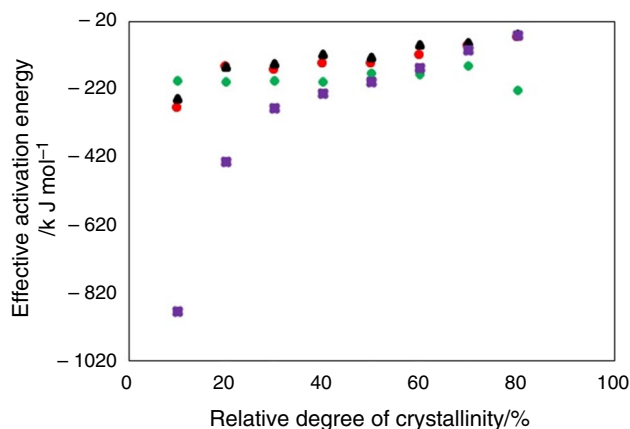

Fig. 9 Dependence of effective activation energy on relative crystallinities for PP, PPG, PPH and PPGH composites. Purple square marker curve represents PP, green diamond marker curve represents PPG, black triangle marker curve represents PPH, and red circle dot marker curve represents PPGH composite system. (Color figure online)

Table 3 ΔE at different % of relative crystallinity by Friedman method

Relative crystallinity /%	ΔE/kJ mol^{-1}			
	PP	PPG	PPH	PPGH
10	− 874	− 194	− 247	− 275
20	− 434	− 198	− 155	− 155
30	− 275	− 195	− 145	− 163
40	− 230	− 198	− 118	− 144
50	− 198	− 173	− 126	− 145
60	− 156	− 175	− 89	− 121
70	− 102	− 150	− 83	− 92
80	− 60	− 222	− 56	− 65
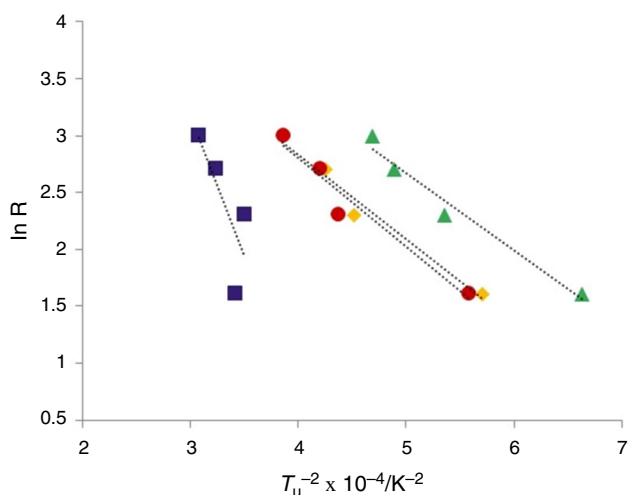
Fig. 10 Nucleation activity plots of lnR versus $1/T_u^2$ for PP, PPG, PPH and PPGH composites. Blue squared marker curve refers to PP, green triangle marker curve refers to PPG, red dot marker curve refers to PPH, and yellow diamond marker curve refers to PPGH composite. (Color figure online)

straightforward compared to the later stages where polymer chains are restrained at high relative degrees of crystallinity [55, 56].

In the case of PPG, a lower trend is observed in the effective activation energy at a relative crystallinity of above 70%. This shows that in the secondary crystallization stage that involves only reorganization of the crystal structures, and a lower amount of activation energy is required to attain % crystallization higher than 70. Between the nanoscale and multiscale composites, the latter (PPGH) shows a lower effective energy barrier than the former (PPH) indicating crystallization is favoured in the presence of multiscale fillers, compared to just nanofillers in PP [57].

Nucleation activity

The nucleation activity plot in Fig. 10 is obtained by plotting ln R versus $1/T_u^2$ where R is the cooling rate and T_u is the undercooling/supercooling temperature (K), i.e. $T_m - T_c$ where T_m is melting temperature, and T_c is crystallization temperature.

The nucleation activity plot provides information about the nucleating effect of the filler on the base material [58]. Dobreva et al. [59] described nucleating activity by the following equation [60].

$$\log R = C - \frac{B}{2.3\Delta T_u^2} \tag{18}$$

where C is a constant and parameter B is defined as

$$B = \frac{\omega\sigma^3 V_m^2}{3NkT_m\Delta S_m^2} \tag{19}$$

where k is Boltzmann constant, T_m is melting temperature, V_m is the molar volume of crystallizing substance, ΔS_m is the molar entropy of mixing σ is the specific surface energy of the spherulites, ω is a geometrical factor, and N is the number of molecules. Nucleating activity is defined as "the ratio of thermodynamic work of formation of 3-D nuclei", represented as $= \frac{B^*}{B}$. B^* and B can be obtained by the slopes of the linear portions of the curves [60]. B is obtained from the neat PP curve, and B^* values are obtained from the filled PP curves. From Table S7, it is observed that B^* values of the filled composites are lower than that of PP. The Φ value ranges from 0 to 1. The closer it is to 0, the higher is the nucleating effect of the filler and thus, higher is the number of nucleation sites. Dobreva et al. [59] concluded that in the range of $1 > \Phi > 0$ sporadic formation of three-dimensional nucleation takes place. Since PPGH has the lowest Φ value, it also has the highest amount of nucleation sites. The physical significance of this result is understood by examining the interface between the polymer matrix and the reinforcements. The presence of both micro- and nanofillers in multiscale composites increases the overall fibre surface area with the PP matrix. Consequently, there is an increase in the interlocking of the fibres and the matrix, which results in a large number of nucleation sites [61]. This contributes to the exceptional physical properties mentioned by Jenifer et al. [7] for multiscale composites. One of the undesirable effects of the incorporation of nanofillers is agglomeration which ultimately inhibits nucleation. The high Φ value of PPH relative to that of PPGH can be attributed to this effect.

XRD analysis

Depending on the conditions under which crystallization occurs, PP crystallizes into different polymorphisms—monoclinic (α), trigonal (β), triclinic (γ) and in some cases metamorphic (smectic), all of which differ in the arrangement of the polymeric chains [62]. It is known from the diffraction spectra of PP that the α peaks (for the monoclinic crystals) are visible at 14°, 17°, 18.5°, 21°, and 22°. The corresponding lattice planes to these Bragg reflections are (110), (040), (130), (111), and (131 + 041). β peaks are visible at 16° (300), and 21° (301), while those for the triclinic crystals (γ) occur at 20.05° (117). Although there are peaks that are visible at 25.5° (060), and 28.5°(220) representative of the monoclinic phase, these reflections do not represent any significant modification and are thus not of importance [63].

The size of the crystallites can be calculated using the Debye–Scherrer equation [63, 64].

$$L_{\text{hkl}} = \frac{k\lambda}{\beta_{\text{hkl}}\cos\theta_{\text{hkl}}} \qquad (20)$$

where L_{hkl}(nm) is the size of ordered crystalline domains, λ (nm) is the X-Ray wavelength, k is a shape factor constant in the range of 0.8–1.2, and β_{hkl} is the full width at half maxima obtained from the peaks at respective 2θ angles. For the purpose of this study, k is assumed to be 0.9 [64]. In this study, the peaks of neat PP were observed at 13.9°, 18.4°, 21.02°, 25.24°, and 28.25° all of which are indicative of the α-crystal which is the most stable and common form. The crystallite sizes obtained for these respective peaks were 16.2 nm, 15.6 nm, 13.4 nm, 15.7 nm, and 9.7 nm. A peak corresponding to the plane (300) at 16.7° can be indicative of the presence of the β crystal, and the crystallite size in this case is 30.03 nm. This peak is visible in PPG, PPH, and PPGH at 15.9°, 16.7° and 16.7° with reducing crystallite sizes of 23.58 nm, 14.64 nm, and 5.65 nm, respectively.

As shown Fig. 11, with the addition of glass fibre alone, there is a significant decrease in the intensity and sharpness of the peaks which occur at 13.9°, 18.4°, 21.35°, 25.37°, and 28.26°, corresponding to crystallite sizes of 11.9 nm, 8.3 nm, 5.6 nm, 14 nm, and 9.2 nm, respectively. The decrease in the intensity of the peaks for PPG can be attributed to the destructive effect the glass fibre has on the crystallization of polypropylene.

With the addition of halloysite nanotubes by 2.5 mass% to PP, the peaks corresponding to PPH are higher in intensity and sharper than PPG. The peaks appear at 13.9°, 18.36° and 20.9° mainly, along with 25.42° and 28.45°, and the corresponding crystallite sizes are 14.2 nm, 13.0 nm, 15.2 nm, 9.3 nm, 10.6 nm, and 10.4 nm. The increase in intensity is attributed to a relatively higher number of crystalline structures and a narrower distribution of the same, at each
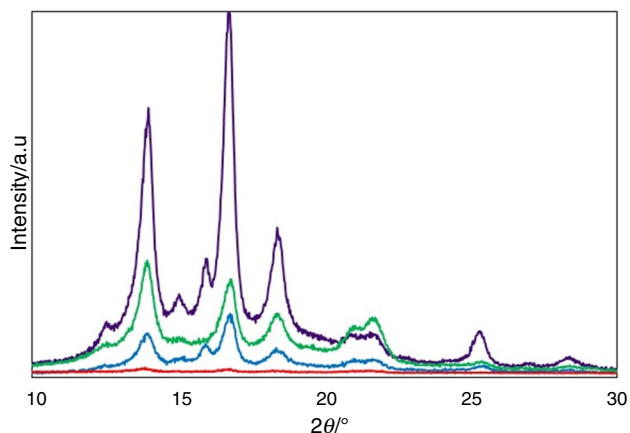
respective plane, whereas the broadening of the same peaks in PPG means lesser number of structures and a larger distribution [6]. A larger distribution indicates a larger range in the crystallite sizes, and this is in line with broad peaks. The slight increase in intensity for PPH can also be indicative of the growth of large crystallites which is reflected in the difference in crystallite sizes of PPH and PPG.

In the case of PPGH, the peaks are the broadest of all and occur visibly at 13.91°, 16.71°, and 21.51° with corresponding crystallite sizes as 17 nm, 5.6 nm and 6.1 nm. This can be explained by two phenomena—the broadening of α peaks due to smaller crystallite sizes and the presence of β crystals due to the last two peaks. Hence, PPGH possesses the smallest crystallite sizes of all with most of them in the trigonal phase and the largest distribution of sizes with an unaltered high level of percent crystallinity [65]. This has immense significance, since it has been shown that the β crystals have improved ductility and impact strength. Owing to the unique surface morphology of HNTs, they possess dual nucleating ability leading to the formation of both α and β type crystals [11]. Thus, it can be concluded from this analysis that while the incorporation of fillers such as glass fibre and halloysite nanotubes has not altered the standard lattice planes of PP, it has increased the number of nucleating sites and reduced the crystallite sizes. Upon comparing the peaks of neat PP with that of the filled composites, the peaks appear at roughly the same 2θ angles, indicating that the addition of reinforcement brings no significant difference in the crystal lattice of PP.

Conclusions

The study on non-isothermal crystallization kinetics of polypropylene reinforced with glass fibres and halloysite nanotubes yielded the following conclusions.

Fig. 11 XRD analysis of PP, PPG, PPGH and PPH samples. Purple curve refers to PP, blue curve refers to PPG, green curve refers to PPH, and red curve refers to PPGH composite. (Color figure online)

- Kinetic study was conducted using different theoretical models, namely Avrami, Ozawa, Mo and Friedman models. The result from the Avrami study suggests that PPGH and PPH have similar crystallization rate constants, the consequence of which is increased rate of crystallization compared to PPG and neat PP. At the same cooling rate, the Z_C value for PPH was the highest, with regard to other composites. The n value ranging from 1 to 2 was indicative of instantaneous crystallization. The Avrami plots exhibited linearity in the initial stage and then proceeded to deviate from linearity. From this result, it can be concluded that the Avrami model is best suited for primary nucleation only.
- Ozawa model was found to be not suitable for the micro and nanocomposite but exhibited a good fit in the case of hybrid composite. Out of the three theoretical mod-

els, the Mo model was best suited for the current system. The decreasing trend of α ratio in nano and hybrid composites signified faster crystallization process. The increasing trend of the same in PPG is counteracted by halloysite nanotubes in PPGH and PPH. Higher values of $F(T)$ suggested the possibility of a complex crystallization process in PPGH. The conformation to the Mo model is high at high percent relative crystallinity, and with the R^2 values of the plots being extremely close to 1, it implied an almost perfect fit.

- Friedman analysis described the dependence of effective activation energy on the extent of relative crystallization of the samples. PPGH exhibited lower effective energy barrier than PPH, indicating crystallization is more favoured in the presence of multiscale fillers. Computation of ϕ from the nucleation activity plot yields the result that PPGH has the highest amount of nucleation sites. This is justified by the high fibre surface area due to the presence of both nano- and microfillers. The low ϕ value of PPH is indicative of agglomeration of the nanotubes.

- In XRD analysis with the addition of GF, there was a significant reduction in the intensity and crystallite size in contrast to the PPH composites where the reduction in the intensity was to a lower extent indicating that HNT had a role in inducing larger number of nucleating sites, leading to bigger crystallite sizes. When both GF and HNT were incorporated into PP, the peaks were broadened to the largest extent hence possessing the smallest crystallite sizes, some of which represented β crystals thus indicating the ability of HNTs to promote β crystal formation.

Declarations

Conflict of interest None declared.

References

1. Campbell D, Qayyum MM. Melt crystallization of polypropylene: effect of contact with fiber substrates. J Polym Sci Polym Phys Ed. 1980;18:83–93. https://doi.org/10.1002/pol.1980.180180107.
2. Gupta AK, Gupta VB, Peters RH, Harland WG, Berry JP. The effect of addition of high-density polyethylene on the crystallization and mechanical properties of polypropylene and glass-fiber-reinforced polypropylene. J Appl Polym Sci. 1982;27:4669–86. https://doi.org/10.1002/app.1982.070271214.
3. Maurya AK, Manik G. Advances towards development of industrially relevant short natural fiber reinforced and hybridized polypropylene composites for various industrial applications: a review. J Polym Res. 2023;30:47. https://doi.org/10.1007/s10965-022-03413-8.
4. Rasana N, Jayanarayanan K, Pegoretti A. Non-isothermal crystallization kinetics of polypropylene/short glass fibre/multiwalled carbon nanotube composites. RSC Adv. 2018;8:39127–39. https://doi.org/10.1039/c8ra07243d.
5. Jayan JS, Deeraj BDS, Saritha A, Joseph K. Theoretical modelling of kinetics of glass transition temperature of PEG toughened epoxy. Plast Rubber Compos. 2020;49:237–44. https://doi.org/10.1080/14658011.2020.1732124.
6. Rasana N, Jayanarayanan K, Pavithra R, Nandhini GR, Ramya P, Veeraraagavan AV. Mechanical and thermal properties modeling, sorption characteristics of multiscale (multiwalled carbon nanotubes/glass fiber) filler reinforced polypropylene composites. J Vinyl Addit Technol. 2019;25(s2):E94-107. https://doi.org/10.1002/vnl.21696.
7. Jenifer A, Rasana N, Jayanarayanan K. Synergistic effect of the inclusion of glass fibers and halloysite nanotubes on the static and dynamic mechanical, thermal and flame retardant properties of polypropylene. Mater Res Express. 2018;5:065308. https://doi.org/10.1088/2053-1591/aac67d.
8. Wang B, Zhang H-R, Huang C, Xiong L, Luo J. Study on non-isothermal crystallization behavior of isotactic polypropylene/bacterial cellulose composites. RSC Adv. 2017;7:42113–22. https://doi.org/10.1039/C7RA07731A.
9. Du M, Guo B, Jia D. Newly emerging applications of halloysite nanotubes: a review. Polym Int. 2010;59:574–82. https://doi.org/10.1002/pi.2754.
10. Du M, Guo B, Wan J, Zou Q, Jia D. Effects of halloysite nanotubes on kinetics and activation energy of non-isothermal crystallization of polypropylene. J Polym Res. 2010;17:109–18. https://doi.org/10.1007/s10965-009-9296-5.
11. Liu M, Guo B, Du M, Chen F, Jia D. Halloysite nanotubes as a novel β-nucleating agent for isotactic polypropylene. Polymer (Guildf). 2009;50:3022–30. https://doi.org/10.1016/j.polymer.2009.04.052.
12. Oburoğlu N, Ercan N, Durmus A, Kaşgöz A. Effects of halloysite nanotube on the mechanical properties and nonisothermal crystallization kinetics of poly (butylene terephthalate)(PBT). J Macromol Sci Part B. 2012;51:860–79. https://doi.org/10.1080/00222348.2011.610231.
13. Zhang Z, Chen J, Liu H, Xiao C. Applicability of Kissinger model in nonisothermal crystallization assessed using a computer simulation method. J Therm Anal Calorim. 2014;117:783–7. https://doi.org/10.1007/s10973-014-3751-1.
14. Zhang S, Wu T, Wang Z, Han J, Guo B, Xu J. Quantitative contribution of each component to secondary nucleation in the blends of homopolymer and its random copolymers. Polymer (Guildf). 2022;245:124735. https://doi.org/10.1016/j.polymer.2022.124735.
15. While I, Hoffman L, Lauritzen-hoffman T. Chapter 2 Polymer Crystallization – Literature review, Cryst. Morphol. Therm.

Stab. Adhes. Prop. Nov. High Perform. Semicrystalline Polyimides, (1999) 29–79. http://scholar.lib.vt.edu/theses/available/etd-051799-162256/

16. Taraghi I, Fereidoon A, Zamani M, Mohyeddin A. Mechanical, thermal, and viscoelastic properties of polypropylene/glass hybrid composites reinforced with multiwalled carbon nanotubes. J Compos Mater. 2015;1211:20–1. https://doi.org/10.1177/0021998314567697.

17. Razavi-Nouri M. Effect of single-walled carbon nanotubes on non-isothermal crystallization kinetics of polypropylene: comparison of Ozawa and Cazé-Chuah methods, Iran. J Polym Sci Technol. 2009;22:53–61. https://doi.org/10.22063/jipst.2009.692.

18. Pérez-Camargo RA, Liu G-M, Wang D-J, Müller AJ. Experimental and data fitting guidelines for the determination of polymer crystallization kinetics. Chin J Polym Sci. 2022;40:658–91. https://doi.org/10.1007/s10118-022-2724-2.

19. Hao W, Yang W, Cai H, Huang Y. Non-isothermal crystallization kinetics of polypropylene/silicon nitride nanocomposites. Polym Test. 2010;29:527–33. https://doi.org/10.1016/j.polymertesting.2010.03.004.

20. Ferreira CI, Dal Castel C, Oviedo MAS, Mauler RS. Isothermal and non-isothermal crystallization kinetics of polypropylene/exfoliated graphite nanocomposites. Thermochim Acta. 2013;553:40–8. https://doi.org/10.1016/j.tca.2012.11.025.

21. Liu S, Yu Y, Cui Y, Zhang H, Mo Z. Isothermal and nonisothermal crystallization kinetics of nylon-11. J Appl Polym Sci. 1998;70:2371–80. https://doi.org/10.1002/(SICI)1097-4628(19981219)70:12%3c2371::AID-APP9%3e3.0.CO;2-4.

22. Coburn N, Douglas P, Kaya D, Gupta J, McNally T. Isothermal and non-isothermal crystallization kinetics of composites of poly(propylene) and MWCNTs. Adv Ind Eng Polym Res. 2018;1:99–110. https://doi.org/10.1016/j.aiepr.2018.06.001.

23. Sruthi S, Abhilash R, Tharun K, Gopi Krishna P, Jayanarayanan K, Rasana N. Experimental and theoretical investigation on the non-isothermal crystallization kinetics of polypropylene reinforced with multiwalled carbon nanotubes. Mater Today Proc. 2019;33:2264–73. https://doi.org/10.1016/j.matpr.2020.04.137.

24. Durmus A, Yalçınyuva T. Effects of additives on non-isothermal crystallization kinetics and morphology of isotactic polypropylene. J Polym Res. 2009;16(2009):489–98. https://doi.org/10.1007/s10965-008-9252-9.

25. Oommen Z, Groeninckx G, Thomas S. Dynamic mechanical and thermal properties of physically compatiblized natural rubber/ poly(methyl methacrylate) blends by the addition of natural rubber-graft-pol(methyl methacrylate). J Polym Sci Part B Polym Phys. 2000;38:525–36. https://doi.org/10.1002/(SICI)1099-0488(20000215)38:4%3c525::AID-POLB4%3e3.0.CO;2-T.

26. Sattari M, Mirsalehi SA, Khavandi A, Alizadeh O, Naimi-Jamal MR. Non-isothermal melting and crystallization behavior of UHMWPE/SCF/nano-SiO$_2$ hybrid composites. J Therm Anal Calorim. 2015;122:1319–30. https://doi.org/10.1007/s10973-015-5003-4.

27. Pengfei N, Xiaojun W, Baoying L, Shengru L, Jie Y. Melting and nonisothermal crystallization behavior of polypropylene/hemp fiber composites. J Compos Mater. 2012;46:203–10. https://doi.org/10.1177/0021998311410.

28. An Y, Wang S, Li R, Shi D, Gao Y, Song L. Effect of different nucleating agent on crystallization kinetics and morphology of polypropylene. E-Polymers. 2019;19:32–9. https://doi.org/10.1515/epoly-2019-0005.

29. Huang C-W, Yang T-C, Hung K-C, Xu J-W, Wu J-H. The effect of maleated polypropylene on the non-isothermal crystallization kinetics of wood fiber-reinforced polypropylene composites. Polymers (Basel). 2018;10:382. https://doi.org/10.3390/polym10040382.

30. Xu W, Ge M, He P. Nonisothermal crystallization kinetics of polypropylene/montmorillonite nanocomposites. J Polym Sci Part B Polym Phys. 2002;40:408–14. https://doi.org/10.1002/polb.10101.

31. Jeziorny A. Parameters characterizing the kinetics of the non-isothermal crystallization of poly(ethylene terephthalate) determined by DSC. Polymer (Guildf). 1978;19:1142–4. https://doi.org/10.1016/0032-3861(78)90060-5.

32. Peneva Y, Valcheva M, Minkova L, Mičušík M, Omastová M. Nonisothermal crystallization kinetics and microhardness of PP/CNT composites. J Macromol Sci Part B. 2008;47:1197–210. https://doi.org/10.1080/00222340802403420.

33. Balsamo V, Urdaneta N, Pérez L, Carrizales P, Abetz V, Müller AJ. Effect of the polyethylene confinement and topology on its crystallisation within semicrystalline ABC triblock copolymers. Eur Polym J. 2004;40:1033–49. https://doi.org/10.1016/j.eurpolymj.2004.01.009.

34. Müller AJ, Balsamo V, Arnal ML. Nucleation and crystallization in diblock and triblock copolymers. Block Copolym. 2005;II:1–63. https://doi.org/10.1007/12_001.

35. Meng Z, Yang L, Geng W, Yao Y, Wang X, Liu Y. Kinetic study on the isothermal and nonisothermal crystallization of monoglyceride organogels. Sci World J. 2014. https://doi.org/10.1155/2014/149753.

36. Ong MY, Chow WS. Kinetics of crystallization for polypropylene/polyethylene/halloysite nanotube nanocomposites. J Thermoplast Compos Mater. 2020;33:451–63. https://doi.org/10.1177/0892705718807.

37. Su C, et al. Crystallization kinetics of poly(ethylene oxide) under confinement in nanoporous alumina studied by in situ X-ray scattering and simulation. Langmuir. 2019;35:11799–808. https://doi.org/10.1021/acs.langmuir.9b01968.

38. Michell RM, Mueller AJ. Confined crystallization of polymeric materials. Prog Polym Sci. 2016;54:183–213. https://doi.org/10.1016/j.progpolymsci.2015.10.007.

39. Layachi A, Frihi D, Satha H, Seguela R, Gherib S. Non-isothermal crystallization kinetics of polyamide 66/glass fibers/carbon black composites. J Therm Anal Calorim. 2016;124:1319–29. https://doi.org/10.1007/s10973-016-5286-0.

40. Kocic N, Kretschmer K, Bastian M, Heidemeyer P. The influence of talc as a nucleation agent on the nonisothermal crystallization and morphology of isotactic polypropylene: the application of the Lauritzen-Hoffmann, Avrami, and Ozawa theories. J Appl Polym Sci. 2012;126:1207–17.

41. Vyazovkin S. Isoconversional kinetics of polymers: the decade past. Macromol Rapid Commun. 2017;38:1600615. https://doi.org/10.1002/marc.201600615.

42. Xu J, Li K, Deng H, Lv S, Fang P, Liu H, Shao Q, Guo Z. Preparation of MCA-SiO$_2$ and its flame retardant effects on glass fiber reinforced polypropylene. Fibers Polym. 2019;20:120–8. https://doi.org/10.1007/s12221-019-8284-6.

43. Guo J, Liu M, Wang H, Yu Y. Non-isothermal crystallization kinetics of polypropylene/bamboo fiber/nano-TiO$_2$ composites. Polym Compos. 2021;42:2531–43. https://doi.org/10.1002/pc.25999.

44. Wu D, Sun Y, Wu L, Zhang M. Linear viscoelastic properties and crystallization behavior of multi-walled carbon nanotube/polypropylene composites. J Appl Polym Sci. 2008;108:1506–13. https://doi.org/10.1002/app.27793.

45. Balta Calleja FJ, Santa Cruz C, Sawatari C, Asano T. New aspects of the microstructure of polyethylene-isotactic polypropylene gel blends as revealed by microhardness: influence of composition. Macromolecules. 1990;23:5352–5. https://doi.org/10.1021/ma00228a008.

46. Chuah KP, Gan SN, Chee KK. Determination of Avrami exponent by differential scanning calorimetry for non-isothermal

crystallization of polymers. Polymer (Guildf). 1999;40:253–9. https://doi.org/10.1016/S0032-3861(98)00188-8.

47. Caze C, Devaux E, Crespy A, Cavrot JP. A new method to determine the Avrami exponent by dsc studies of non-isothermal crystallization from the molten state. Polymer (Guildf). 1997;38:497–502. https://doi.org/10.1016/S0032-3861(96)00552-6.

48. McFerran NLA, Armstrong CG, McNally T. Nonisothermal and isothermal crystallization kinetics of nylon-12. J Appl Polym Sci. 2008;110:1043–58. https://doi.org/10.1002/app.28696.

49. Van Krevelen DW, Te Nijenhuis K. Properties of polymers: their correlation with chemical structure; their numerical estimation and prediction from additive group contributions. Amsterdam: Elsevier; 2009.

50. Vyazovkin S. Kissinger method in kinetics of materials: things to beware and be aware of. Molecules. 2020;25:2813. https://doi.org/10.3390/molecules25122813.

51. Friedman HL. Kinetics of thermal degradation of char-forming plastics from thermogravimetry. Application to a phenolic plastic. J Polym Sci Part C Polym Symp. 1964;6:183–95.

52. Vassiliou AA, Papageorgiou GZ, Achilias DS, Bikiaris DN. Non-isothermal crystallisation kinetics of in situ prepared poly(ε-caprolactone)/surface-treated SiO_2 nanocomposites. Macromol Chem Phys. 2007;208:364–76. https://doi.org/10.1002/macp.200600447.

53. Kalkar AK, Deshpande VD, Vatsaraj BS. Isoconversional kinetic analysis of DSC data on nonisothermal crystallization: Estimation of Hoffman–Lauritzen parameters and thermal transitions in PET/MMT nanocomposites. Polymer (Guildf). 2014;55:6948–59. https://doi.org/10.1016/j.polymer.2014.10.068.

54. Sbirrazzuoli N. Interpretation and physical meaning of kinetic parameters obtained from isoconversional kinetic analysis of polymers. Polymers (Basel). 2020;12:1280. https://doi.org/10.3390/polym12061280.

55. Jhu Y-S, Yang T-C, Hung K-C, Xu J-W, Wu T-L, Wu J-H. Nonisothermal crystallization kinetics of acetylated bamboo fibre-reinforced polypropylene composites. Polymers (Basel). 2019;11:1078. https://doi.org/10.3390/polym11061078.

56. Qu D, Cai J, Huang F, Zhang J, Zuo H, Sun S, Liu J, Bai Y. High-performance optical PET analysis via non-isothermal crystallization kinetics. Polymers. 2022;14:3044. https://doi.org/10.3390/polym14153044.

57. Samantaray SK, Satapathy BK. On the crystal growth kinetics of ultra-toughened biobased polyamide 410: new insights on dynamic crystallization. J Appl Polym Sci. 2022;139:51494. https://doi.org/10.1002/app.51494.

58. Cai Y, Yan S, Fan Y, Yu Z, Chen X, Yin J. The nucleation effect of N, N′-bis (benzoyl) alkyl diacid dihydrazides on crystallization of biodegradable poly (l-lactic acid), Iran. Polym J. 2012;21:435–44. https://doi.org/10.1007/s13726-012-0046-x.

59. Dobreva A, Gutzow I. Activity of substrates in the catalyzed nucleation of glass-forming melts. II. Experimental evidence. J Non Cryst Solids. 1993;162:13–25. https://doi.org/10.1016/0022-3093(93)90737-I.

60. Papageorgiou GZ, Achilias DS, Bikiaris DN, Karayannidis GP. Crystallization kinetics and nucleation activity of filler in polypropylene/surface-treated SiO_2 nanocomposites. Thermochim Acta. 2005;427:117–28. https://doi.org/10.1016/j.tca.2004.09.001.

61. Mittal G, Rhee KY, Mišković-Stanković V, Hui D. Reinforcements in multi-scale polymer composites: processing, properties, and applications. Compos Part B Eng. 2018;138:122–39. https://doi.org/10.1016/j.compositesb.2017.11.028.

62. Jayanarayanan K, Thomas S, Joseph K. In situ microfibrillar blends and composites of polypropylene and poly (ethylene terephthalate): morphology and thermal properties. J Polym Res. 2011;18:1–11.

63. Machado G, Denardin EL, Kinast EJ, Gonçalves MC, De Luca MA, Teixeira SR, Samios D. Crystalline properties and morphological changes in plastically deformed isotatic polypropylene evaluated by X-ray diffraction and transmission electron microscopy. Eur Polym J. 2005;41:129–38. https://doi.org/10.1016/j.eurpolymj.2004.08.011.

64. Bishnoi A, Kumar S, Joshi N. Wide-angle X-ray diffraction (WXRD): technique for characterization of nanomaterials and polymer nanocomposites. In: Microscopy methods in nanomaterials characterization, Elsevier, 2017, 313–337. https://doi.org/10.1016/B978-0-323-46141-2.00009-2

65. Wang Y, Cheng L, Cui X, Guo W. Crystallization behavior and properties of glass fiber reinforced polypropylene composites. Polymers (Basel). 2019;11:1198. https://doi.org/10.3390/polym11071198.